


## Prediction of quaternary hydrides based on densest ternary sphere packings

Ryotaro Koshiji<sup>①,\*</sup>, Masahiro Fukuda<sup>②,†</sup>, Mitsuaki Kawamura<sup>③,‡</sup> and Taisuke Ozaki<sup>④,§</sup>  
*Institute for Solid State Physics, The University of Tokyo, Kashiwa 277-8581, Japan*

 (Received 13 June 2022; accepted 20 October 2022; published 7 November 2022)

We exhaustively search quaternary metal hydrides based on the (13-2-1) and (13-3-1) structures that are two of the putative densest ternary sphere packings in cubic systems [R. Koshiji *et al.*, *Phys. Rev. E* **104**, 024101 (2021)]. The 73 304 candidate hydrides are generated by substituting the small spheres with hydrogen atoms, and the medium, large, and fourth spheres with metallic atoms. Specifically, the substitution of the small spheres with hydrogen atoms gives the unconventional hydrogen sublattices. We screen unstable hydrides in the candidates through geometrical optimizations, constant pressure molecular dynamics simulations, and phonon calculations under hydrostatic pressure of 10 GPa, and identify 23 hydrides with static and dynamic stability, including  $\text{H}_{12}\text{ScY}_2\text{La}$  and  $\text{H}_{12}\text{TiNi}_3\text{Ba}$ . The superconducting transition temperatures  $T_c$ , calculated by density functional theory for superconductors, are found to be 5.7 and 6.7 K for the selected two hydrides  $\text{H}_{12}\text{ScY}_2\text{Ca}$  and  $\text{H}_{12}\text{ScY}_2\text{Sr}$ , respectively. We expect that the 23 candidates of hydrides screened by the exhaustive search for 73 304 hydrides provide a guideline to narrow down the search space for trials in the experimental synthesis of quaternary metal hydrides.

DOI: [10.1103/PhysRevMaterials.6.114802](https://doi.org/10.1103/PhysRevMaterials.6.114802)

### I. INTRODUCTION

The recent progress of crystal structure prediction methods, including the evolutionary algorithms [1–5], particle swarm-intelligence approach [6–8], and *ab initio* random structure searching approach [9,10], has contributed a great deal to the discovery of novel materials. For example, a considerable number of binary hydrides were successfully predicted, and subsequently several cubic hydrides among them, including  $\text{YH}_6$  and  $\text{LaH}_{10}$  [11,12], were experimentally synthesized as high-temperature superconductors (SCs) under high pressure [13–17]. Furthermore, the prediction of the metastable hydride  $\text{Li}_2\text{MgH}_{16}$ , which was predicted to be a room-temperature SC [18], ignites more interest in seeking possible ternary and quaternary hydrides with high-temperature superconductivity synthesized under mild conditions. However, it remains a big challenge to study ternary and quaternary systems since the size of the chemical and configuration space becomes explosively large for these cases. In fact, the diversity of ternary hydrides makes it difficult to predict high-temperature SCs in spite of great efforts to search ternary hydrides [19–41], while a few high-pressure experiments also found that some ternary hydrides are SCs [42–44].

The hydrogen sublattices in clathrate hydrides such as  $\text{YH}_6$  and  $\text{LaH}_{10}$  are predominantly responsible for high-temperature Bardeen-Cooper-Schrieffer superconductivity since hydrogen has the lightest mass, strong electron-

phonon coupling, and the large electron density of states at the Fermi level, consisting of the degenerate  $1s$  states of hydrogen orbitals due to the high symmetries [45,46]. Note that metallic hydrogen is predicted to be a high-temperature phonon-mediated SC [47,48], but an extremely high pressure of 495 GPa seems to be necessary to synthesize the metal hydrogen [49]. Instead, so-called *chemical compression* from relatively heavier elements can be utilized to stabilize the hydrogen sublattices in clathrate hydrides under a relatively low pressure [46].

A structural feature similar to the hydrogen sublattice in the clathrate hydrides can be found in some of the putative densest ternary sphere packings (PDTSPs); for example, small spheres in the (13-2-1) and (13-3-1) structures shown in Figs. 1(a) and 2(a) have cage structures enclosing the medium and large spheres [50,51]. Note that we name a PDTSP consisting of  $l$  small,  $m$  medium, and  $n$  large spheres per unit cell as  $(l-m-n)$  structure. The structural similarity indicates that the two PDTSPs can be regarded as the structural prototypes for clathrate hydrides. In fact, some of the crystals of the binary hydrides correspond to the putative densest binary sphere packings (PDBSPs) [52]; for example, the crystal of  $\text{LaH}_{10}$  is isotopic to the  $\text{XY}_{10}$  structure shown in Fig. 3(a), and similarly the crystal of  $\text{YH}_6$  is isotopic to the (6-1) structure shown in Fig. 3(b). Furthermore, Zhang *et al.* [40] predicted  $\text{LaBeH}_8$ , where the tetrahedral site is occupied by a tetrahedron consisting of hydrogen atoms. We see a similar local structure in the (10-4-1) structure that is one of the PDTSPs [50]. It is worth pointing out that in general, the PDTSPs tend not to have high symmetries [50–52], but the (13-2-1) and (13-3-1) structures have high symmetries of the  $Fm\bar{3}m$  and  $Pm\bar{3}m$ , respectively, if the small structural distortions are corrected.

In general, the densest sphere packings can be expected as the structural prototypes for crystals, in fact, some of the

\*cosaji@issp.u-tokyo.ac.jp

†masahiro.fukuda@issp.u-tokyo.ac.jp

‡mkawamura@issp.u-tokyo.ac.jp

§t-ozaki@issp.u-tokyo.ac.jp

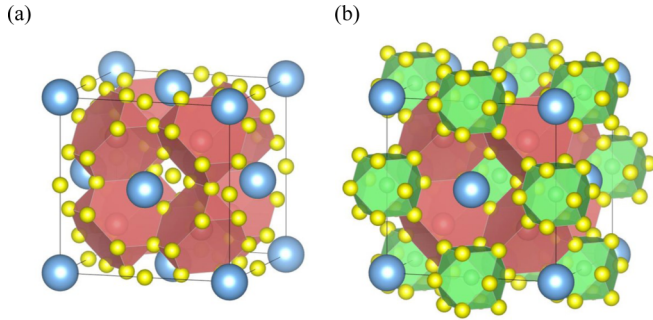


FIG. 1. (a) The (13-2-1) structure [50,51] with the  $Fm\bar{3}m$  symmetry, which is the PDTSP at several radius ratios including 0.44 : 0.64 : 1.00. (b) The (12-1-2-1) structure with the  $Fm\bar{3}m$  symmetry, where one small sphere placed at the center of an octahedral site is substituted by a semismall sphere. In all figures of the paper, the small, medium, and large spheres are represented by yellow, red, and blue balls, respectively, and the green balls correspond to the fourth spheres, named semismall sphere. Note that the color of the polyhedron is the same as that of the center sphere. All the figures are drawn by VESTA [54].

crystals under the ordinary pressure such as  $\text{AlB}_2$ ,  $\text{ThSi}_2$ , and  $\text{UB}_4$ , correspond to the PDBSPs [52]. In addition, the reduction of distances between atoms caused by the high pressure weakens the directional orientation of the bonds due to the strong repulsive force by the Pauli exclusion principle [53]. Therefore, we can expect that the PDTSPs might be the stable prototypes of crystals of the materials that are synthesized at least under extremely high pressures, where the materials have not been exhaustively searched.

In this study, we exhaustively search quaternary hydrides based on the (13-2-1) and (13-3-1) structures, which are used to derive the quaternary structural prototypes by substituting one small sphere in a cluster consisting of 13 small spheres with a fourth sphere. For each PDTSP, 36 652 kinds of compounds are systematically generated by substituting the small spheres with hydrogen atoms, and the medium, large, and fourth spheres with metallic atoms. Thus, we have 73 304 candidate compounds of hydrides in total for the exhaustive search for the stable hydrides under 10 GPa. We screen

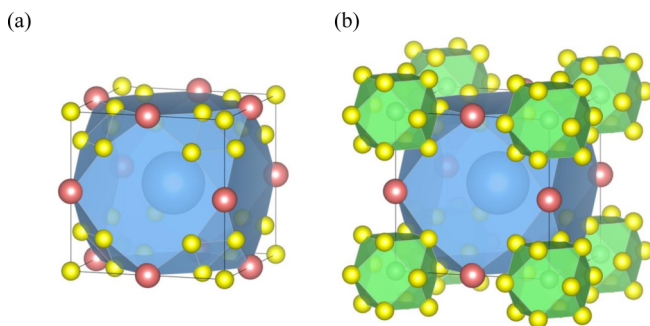


FIG. 2. (a) The (13-3-1) structure with the  $Pm\bar{3}m$  symmetry, which is the PDTSP at the several radius ratios including 0.30 : 0.40 : 1.00. (b) The (12-1-3-1) structure with the  $Pm\bar{3}m$  symmetry, where one small sphere placed at the vertex of the unit cell is substituted by a semismall sphere.

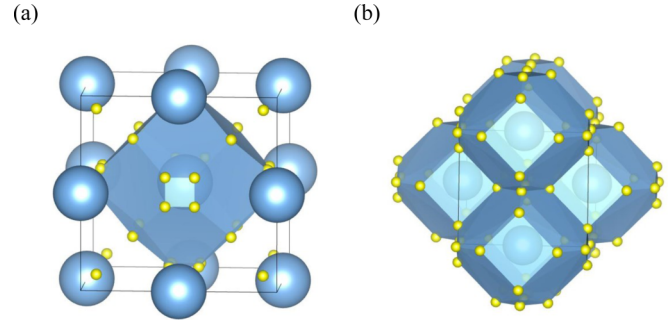


FIG. 3. Two PDBSPs that correspond to the crystals of clathrate hydrides synthesized under high pressure with high- $T_c$  superconductivity. (a) The  $\text{XY}_{10}$  structure [52,55,56], which corresponds to the crystal of  $\text{LaH}_{10}$  [13–16]. (b) The (6-1) structure [52,55,56], which corresponds to the crystal of  $\text{YH}_6$  [17].

unstable hydrides for the candidates through geometrical optimizations, molecular dynamics simulations, and phonon calculations, and identify 23 hydrides with static and dynamic stability, including  $\text{H}_{12}\text{ScY}_2\text{La}$  and  $\text{H}_{12}\text{TiNi}_3\text{Ba}$ .

The paper is organized as follows: Section II describes the conditions for the exhaustive search; Sec. III shows the computational results. In Sec. IV, we summarize this study.

## II. COMPUTATIONAL DETAILS

### A. *Ab initio* simulations

We use the OPENMX code [57–60] to perform density functional theory calculations based on norm-conserving pseudopotentials and optimized pseudoatomic localized basis functions. The exchange-correlation functional was treated within the generalized gradient approximation by Perdew, Burke, and Ernzerhof [61,62]. The pseudoatomic orbital basis functions are detailed in the Supplemental Material [63]. In geometrical optimizations, lattice vectors and internal coordinates are simultaneously optimized without any constraint by quasi-Newton methods [64]. We also perform NVT ensemble molecular dynamics simulations (NVTMD) using the Nosé-Hoover method [65–67], and a constant-temperature and constant-pressure molecular dynamics simulations (NPTMD) using the velocity scaling method [68] and the Parrinello-Rahman method [69]. In the geometrical optimizations, NVTMD, and NPTMD, the  $k$  grids of  $n_1 \times n_2 \times n_3$  for the Brillouin zone sampling are determined based on the lengths  $|\mathbf{g}_i|$  of reciprocal lattice vectors  $\mathbf{g}_i$  ( $\text{\AA}^{-1}$ ) as

$$n_i = \lceil 3|\mathbf{g}_i| \rceil, \quad (1)$$

and the regular mesh of 230 Ry in real space was used for the numerical integration and for the solution of the Poisson equation [59].

To confirm the dynamic stability, we also use the ALAMODE code [70] to calculate the phonon dispersion. The  $k$  grids of  $n_1 \times n_2 \times n_3$  are set to be twice as large as that calculated as Eq. (1), and the regular mesh of 1000 Ry in real space was used for the numerical integration and for the solution of the Poisson equation. In the calculations of force constants, we choose the displacement of 0.1  $\text{\AA}$ , and calculate the force constants after the symmetrization of structures. For the

TABLE I. The list of substitution atoms for spheres, where the symbol E corresponds to empty.

Sphere size	Elements
Small	H
Semismall	E, H, Li, Be, Na, Mg, Al, K, Ca, Sc, Ti, V, Cr, Mn, Fe, Co, Ni, Cu, Zn
Medium	From Li to Hg (except for B to Ne, Si to Ar, Br, Kr, Xe, Ce to Lu, Pt)
Large	From K to Hg (except for Br, Kr, Xe, Ce to Lu, Pt)

face-centered cubic system, the force constants are calculated using the  $2 \times 2 \times 2$  conventional cells, while for the primitive cubic system, they are calculated using the  $3 \times 3 \times 3$  primitive cells.

All the calculations to determine static and dynamic stability are performed under hydrostatic pressure of 10 GPa. In the initial screening process, the spin polarization is not taken into account to reduce the computational cost, while the spin polarization is considered in the final screening process to determine static and dynamic stability. The space groups are determined by the code SPGLIB [71].

### B. Prototype structures and chemical compositions

One of our prototype structures is the (13-2-1) structure [50,51], which has the  $Fm\bar{3}m$  symmetry as shown in Fig. 1(a). The large spheres constitute the fcc structure without contact, and a large sphere is surrounded by 24 small spheres constituting a truncated octahedron. The tetrahedral site is occupied by one medium sphere which is surrounded by 12 small spheres constituting a truncated tetrahedron. The octahedral site is occupied by one small sphere which is surrounded by 12 small spheres constituting a cuboctahedron. The structure is the PDTSP at several radius ratios such as 0.44 : 0.64 : 1.00, at which small and medium spheres are too large to be placed in the tetrahedral and octahedral sites if large spheres comprising the fcc structure contact with each other. Thus, the (13-2-1) structure is not a trivial PDTSP. It should be noted that the cages of small spheres surrounding large spheres is isotypic to the cages of hydrogen atoms in  $\text{LaYH}_{12}$  and  $\text{LaY}_3\text{H}_{24}$  [38].

In the (13-2-1) structure, we can see the clusters consisting of 13 small spheres. However, crystal structures tend to prefer the coordination polyhedron [72]. Therefore, we replace the small sphere at the center of the cluster with metallic atoms so that the metallic atoms should be coordinated by 12 small spheres comprising a cuboctahedron. We call the quaternary structure shown in Fig. 1(b) as the (12-1-2-1) structure. This structure also has the  $Fm\bar{3}m$  symmetry.

The second prototype structure in the study is the (13-3-1) structure [50,51], which has the  $Pm\bar{3}m$  symmetry as shown in Fig. 2(a). The structure, which is the PDTSP at several radius ratios such as 0.30 : 0.40 : 1.00, can be derived by substituting an atom at the vertex of the unit cell of the perovskite structure with a cluster of 13 small spheres. To design the cuboctahedral coordinations of the small sphere at the centers of the clusters, we substitute a small sphere at the center of the cluster of 13 small spheres with a semismall sphere. We call the quaternary structure shown in Fig. 2(b) as the (12-1-3-1) structure. The structure also has the  $Pm\bar{3}m$  symmetry. The small spheres in the structure enclose the semismall, medium, and large spheres.

Table I shows the list of substitution atoms for spheres in the (12-1-2-1) and (12-1-3-1) structures. Small spheres are substituted with only hydrogen atoms. The number of chemical compositions for each structural prototype is 36 652. The initial lattice size of each hydride is determined based on the covalent radii [73] as follows: we estimate how the lattice must be enlarged for each atom to reduce the overlaps, defined by the covalent radii, to zero with near atoms, and determine the size of the initial lattice by calculating the average of them to expand the lattice moderately.

### C. Screening of unstable hydrides

First, we geometrically optimize the initial structures of the candidates under 10 GPa. Next, to exclude the unstable hydrides with small computations, we execute the reoptimizations with adding slight structural distortions. The maximum number of structural optimization steps is set to be 80. Finally, we perform the NVTMD under 10 GPa with a time step of 0.5 fs for 1.0 ps at 200 K in the  $1 \times 1 \times 1$  unit cell. If a hydride transforms a disordered structure, we regard that the hydride is dynamically unstable. In this screening process, we do not take account of the spin polarization to reduce the computational cost.

### D. Standard enthalpies of formations

The standard enthalpy of formation (SEF) is defined by the enthalpy of a material minus the sum of those of elemental materials. If the SEF is positive, the material is less probable to be synthesized. When we calculate the enthalpy of an elemental material under 10 GPa, the crystal structure is set to be isotypic to that under the 0 GPa, i.e., only the lattice size is optimized under a given pressure. We note that the crystal of lanthanum metal is set to be the fcc structure and the spin polarization is taken into account in all the calculations.

### E. Confirmation of structural stabilities

The structural stability is confirmed by phonon dispersion and NPTMD. If a material has no imaginary frequency mode of phonon, we regard that the structure is dynamically stable. The NPTMD is performed under 10 GPa with a time step of 0.5 fs for 0.5 ps at 200 K in the  $2 \times 2 \times 2$  unit cell. Since these calculations need large computational costs, we perform them for some of the hydrides which have lower SEFs and have no spin polarization.

### F. Superconducting transition temperature

We estimate the superconducting transition temperature ( $T_c$ ) by using density functional theory for superconductors

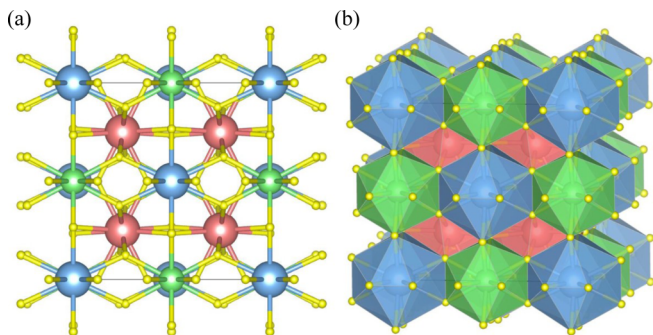


FIG. 4. The conventional cell of  $\text{H}_{12}\text{ScY}_2\text{La}$ . This structure is the variant structure of the  $(12-1-2-1)_V$  structure named  $(12-1-2-1)_V$  structure, and it has the  $Fm\bar{3}$  symmetry. The yellow, green, red, and blue balls correspond to the hydrogen, scandium, yttrium, and lanthanum atoms, respectively. (a) The crystal is shown by balls and sticks. (b) The crystal is shown by polyhedrons consisting of hydrogen atoms.

(SCDFT) [74]. We calculate phonons and electron-phonon coupling using density-functional perturbation theory implemented in QUANTUM ESPRESSO code [75]. For SCDFT calculation, we use the Eliashberg-combined electron-phonon contribution [76], plasmonic effect [77,78], and the spin fluctuation [79] implemented in SUPERCONDUCTING-TOOLKIT [80]. The numerical condition is as follows: Brillouin-zone integration is performed on an  $8^3$  ( $4^3$ ) grid for electronic (phononic) wave number by using the optimized tetrahedron method [81] while the  $16^3$  grid for electronic structure is used for the calculation of the density of states and phonon linewidth. The plane-wave cutoff energy is set to 60 Ry, which is suitable for the standard solid-state pseudopotentials [82]. As a reference, we also calculate  $T_c$  for  $\text{H}_3\text{S}$  at 200 GPa ( $Im\bar{3}m$  phase) with  $9^3$ ,  $18^3$ , and  $36^3$  wave-number grids.

### III. RESULTS AND DISCUSSION

#### A. Stable hydrides

After generating 73 304 candidate compounds derived from the  $(12-1-2-1)$  and  $(12-1-3-1)$  structures, we exclude unstable hydrides by geometrical optimizations and NVTMDs. Among the hydrides that keep symmetric structures in the process, we calculate the phonon dispersions and perform the NPTMDs for 28 hydrides which have the lowest SEFs and exhibit no spin polarization in order to confirm the dynamic stability.

In the NVTMDs, we find that almost all the candidates generated from the  $(12-1-2-1)$  structure do not prefer their original structure but another one with the  $Fm\bar{3}$  symmetry named  $(12-1-2-1)_V$  structure shown in Fig. 4. Among the compounds with the  $(12-1-2-1)_V$  structure, we calculate the phonon dispersions for 18 hydrides which have SEFs less than  $-10.0$  eV/f.u. and exhibit no spin polarization even in the spin-polarized calculations. As a result, we confirm that 16 hydrides listed in Table II are dynamically stable as shown in Figs. 1 and 2 of the Supplemental Material [63]. Tables I and II of the Supplemental Material [63] list the  $(12-1-2-1)_V$ -type hydrides having the SEFs in between  $-10.0$  and  $-5.0$ , and

TABLE II. The 16 kinds of  $(12-1-2-1)_V$ -type hydrides which have SEFs less than  $-10.0$  eV/f.u. and no spin polarization, and show the dynamic stability confirmed by both the phonon calculation and the NPTMD, except for  $\text{H}_{12}\text{ScLa}_2\text{Ba}$  marked by \* for which only the phonon calculation supports the dynamic stability.

SEFs (eV/f.u.)	Material names
-12.20	$\text{H}_{12}\text{ScY}_2\text{La}$
-11.87	$\text{H}_{12}\text{ScSc}_2\text{Y}$
-11.60	$\text{H}_{12}\text{ScY}_2\text{Zr}$
-11.58	$\text{H}_{12}\text{ScY}_2\text{Hf}$
-11.45	$\text{H}_{12}\text{ScSc}_2\text{Hf}$
-11.12	$\text{H}_{12}\text{ScY}_2\text{Ca}$
-11.05	$\text{H}_{12}\text{ScY}_2\text{Sr}$
-10.82	$\text{H}_{12}\text{TiY}_2\text{Ca}$
-10.78	$\text{H}_{12}\text{TiY}_2\text{Sr}$
-10.49	$\text{H}_{12}\text{ScLa}_2\text{Sr}$
-10.26	$\text{H}_{12}\text{ScLa}_2\text{Ba}^*$
-10.15	$\text{H}_{12}\text{CaZr}_2\text{Zr}$
-10.15	$\text{H}_{12}\text{TiLa}_2\text{Sr}$
-10.13	$\text{H}_{12}\text{TiSc}_2\text{Zr}$
-10.12	$\text{H}_{12}\text{TiY}_2\text{Ba}$
-10.00	$\text{H}_{12}\text{TiLa}_2\text{Ba}$

$-5.0$  and  $-1.3$  eV/f.u., respectively, which show the dynamic stability in the NVTMDs and have no spin polarization. In addition, Table III of the Supplemental Material [63] lists the  $(12-1-2-1)_V$ -type hydrides which also show the dynamic stability in the NVTMDs with *spin* polarization. The NPTMDs under 10 GPa also support the results of phonon calculations except for  $\text{H}_{12}\text{ScLa}_2\text{Ba}$ , marked by \* in Table II, exhibiting the dynamic instability in the NPTMD. As an example of the  $(12-1-2-1)_V$  structure, we show the electronic band, the density of state (DOS), and the projected DOS of the hydrogen atoms (H-PDOS) of  $\text{H}_{12}\text{ScY}_2\text{Ca}$  in Fig. 5. We see that  $\text{H}_{12}\text{ScY}_2\text{Ca}$  has a large H-PDOS near the Fermi level. In addition, we show the phonon dispersion, DOS, and the projected phonon-DOS of the hydrogen atoms of  $\text{H}_{12}\text{ScY}_2\text{Ca}$  in Fig. 6. We see that the high phonon frequency modes in  $\text{H}_{12}\text{ScY}_2\text{Ca}$  are comprised of hydrogen atoms, and they are decoupled from the other lower frequency modes by metallic atoms with a large gap. The phonon dispersions and band structures of the other 15 hydrides with the  $(12-1-2-1)_V$  structure are shown in Figs. 1–4 of the Supplemental Material [63].

TABLE III. The six kinds of  $(12-1-3-1)$ -type hydrides which have SEFs less than  $-5.0$  eV/f.u. and no spin polarization, and show the dynamic stability confirmed by both the phonon calculation and the NPTMD, except for  $\text{H}_{12}\text{ScNi}_3\text{La}$  marked by \* for which only the phonon calculation supports the dynamic stability.

SEFs (eV/f.u.)	Material names
-6.47	$\text{H}_{12}\text{TiNi}_3\text{Ba}$
-5.82	$\text{H}_{12}\text{TiNi}_3\text{Sr}$
-5.72	$\text{H}_{12}\text{ScNi}_3\text{La}^*$
-5.69	$\text{H}_{12}\text{ScPd}_3\text{Ba}$
-5.50	$\text{H}_{12}\text{LiRu}_3\text{Ba}$
-5.07	$\text{H}_{12}\text{TiPd}_3\text{Ba}$

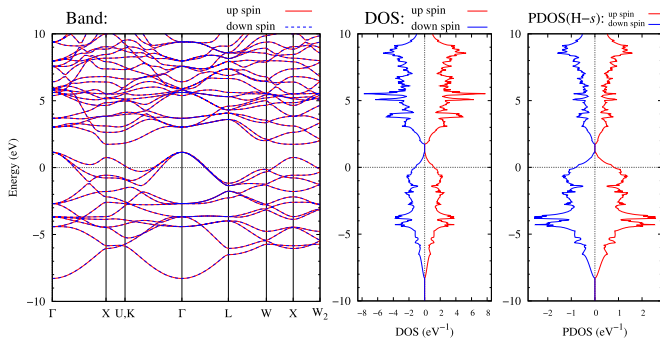


FIG. 5. The bands, the density of state (DOS) per f.u., and the projected DOS of the hydrogen atoms (H-PDOS) of  $H_{12}ScY_2Ca$  under 10 GPa.

In the NVTMDs we see that the original (12-1-2-1) structure is preferred by a few candidate compounds. To further check the dynamic stability of the compounds with the (12-1-2-1) structure, we calculate the phonon dispersions of the four hydrides that have the lowest SEFs in them except for those having spin polarizations and relatively large structural distortions. The result indicates that only  $H_{12}TiSc_2Cs$  shown in Fig. 7 is dynamically stable. The phonon dispersion and electronic band structure are shown in Figs. 5 and 6 of the Supplemental Material [63], respectively. Although the phonon calculations show the dynamic stability of only  $H_{12}TiSc_2Cs$  in the compounds with the original (12-1-2-1) structure, we note that the NPTMDs suggest the dynamic stability of not only  $H_{12}TiSc_2Cs$ , but also  $H_{12}VSc_2Cs$ , which have the SEFs of  $-7.70$  eV/f.u. and  $-6.31$  eV/f.u., respectively.

On the other hand, the (12-1-3-1) structure is preferred in NVTMDs by a considerable number of hydrides including  $H_{12}TiNi_3Ba$  as shown in Fig. 8. Among hydrides with the (12-1-3-1) structure, we calculate the phonon dispersions of six hydrides which have the SEFs less than  $-5.0$  eV/f.u. and exhibit no spin polarization even in the spin-polarized calculations. As a result, all of them, which are listed in Table III, show the dynamic stability as shown in Fig. 7 of the Supplemental Material [63]. The NPTMDs under 10 GPa

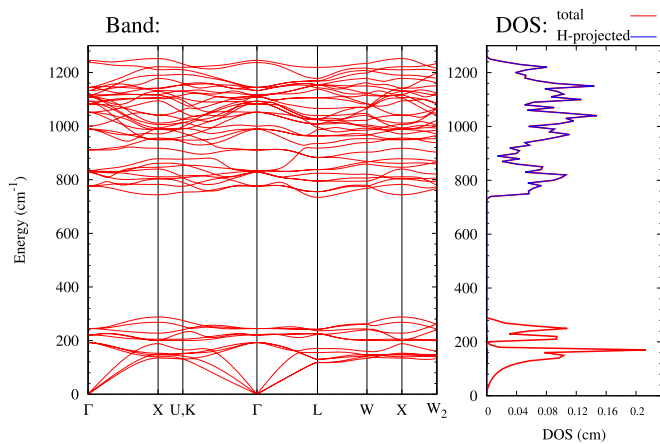


FIG. 6. The phonon dispersions, DOS per f.u., and the projected phonon-DOS of the hydrogen atoms of  $H_{12}ScY_2Ca$  under 10 GPa.

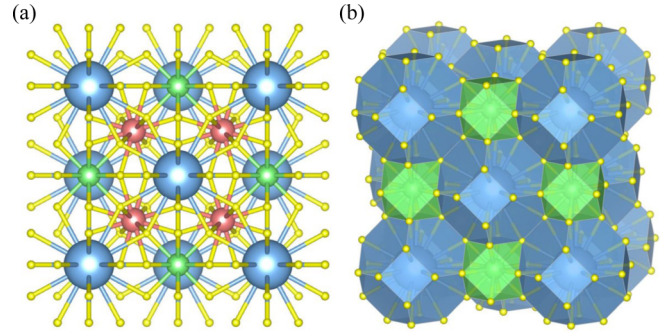


FIG. 7. The conventional cell of the  $H_{12}TiSc_2Cs$ . The yellow, green, red, and blue balls correspond to the hydrogen, titanium, scandium, and cesium atoms, respectively.

also support the results of phonon calculations except for  $H_{12}ScNi_3La$ , marked by \* in Table III, exhibiting the dynamic instability in the NPTMD. The electronic band structures of the (12-1-3-1)-type hydrides listed in Table III are shown in Fig. 8 of the Supplemental Material [63], which show that all the hydrides are metal. In addition to Table III, Table IV of the Supplemental Material [63] lists the (12-1-3-1)-type hydrides which show the dynamic stability in the NVTMDs, and have the SEFs more than  $-5.0$  eV/f.u. and no spin polarization. Also, Table V of the Supplemental Material [63] lists the (12-1-3-1)-type hydrides which also show the dynamic stability in NVTMDs but exhibit *spin* polarizations.

The website [83] gives all the three-dimensional data of the hydrides listed in Tables II and III, and Tables I, II, III, IV, and V of the Supplemental Material [63],  $H_{12}TiSc_2Cs$  and  $H_{12}VSc_2Cs$  of the (12-1-2-1)-type hydrides.

Note that as listed in Table I, we also substitute semismall spheres with hydrogen atoms or empty; however, our calculations suggest that such ternary hydrides are less probable to be synthesized at least under 10 GPa.

### B. Thermodynamic stability of hydrides

The SEFs under 10 GPa of the four kinds of decomposition paths from  $H_{12}ScY_2Ca$ :

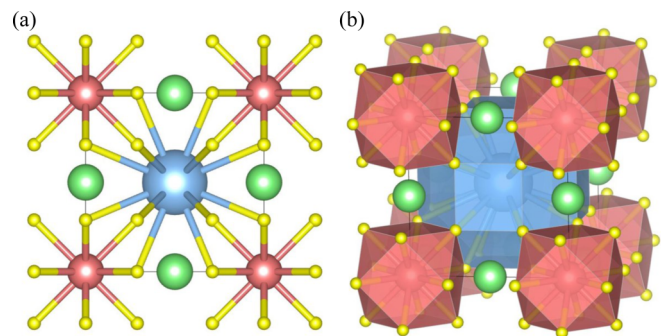
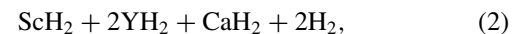
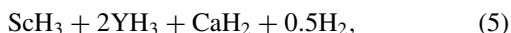
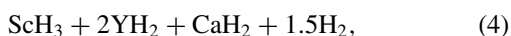
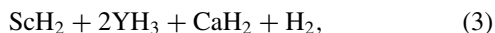


FIG. 8. The primitive cell of  $H_{12}TiNi_3Ba$ . The yellow, green, red, and blue balls correspond to the hydrogen, titanium, nickel, and barium atoms, respectively.

TABLE IV. The density of states per atom and per spin, electron-phonon mass-enhancement factor, averaged phonon frequency, and  $T_c$  without (wo) and with (w) spin fluctuation (SF) for two stable metallic quaternary hydrides and  $H_3S$  in the  $Im\bar{3}m$  phase at 200 GPa.

	$H_{12}ScY_2Ca$	$H_{12}ScY_2Sr$	$H_3S$
$D(\varepsilon_F)$ (/eV/atom/spin)	0.076	0.079	0.079
$\lambda$	0.65	0.68	2.73
$\omega_{ln}$ (K)	591	550	1248
$T_c$ (wo/SF) (K)	10.6	11.5	203
$T_c$ (w/SF) (K)	5.7	6.7	190



are  $-11.11$ ,  $-12.26$ ,  $-11.23$ , and  $-12.38$  eV/f.u., respectively. We referred to the Materials Project [84] to obtain the initial structural data of  $ScH_2$ ,  $ScH_3$ ,  $YH_2$ ,  $YH_3$ , and  $CaH_2$ . The computational details are discussed in the Supplemental Material [63]. Since the SEF of  $H_{12}ScY_2Ca$  under 10 GPa is  $-11.12$  eV/f.u., the quaternary hydride is less stable than the decompositions of Eqs. (3) and (5) by about 1.2 eV/f.u., corresponding to the thermodynamic instability of 78.6 meV/atom compared to the case of Eq. (5).

Although  $H_{12}ScY_2Ca$  under 10 GPa does not have the lowest enthalpy, it will keep the  $Fm\bar{3}$  structure unless it is disturbed sufficiently to reconstruct the most stable network of atoms. In fact,  $H_{12}ScY_2Ca$  are considerably stable since it has almost the same enthalpy as the decomposition of Eqs. (2) and (4). Generally, the 23 hydrides may not be the most stable structure under 10 GPa, but our calculations imply that they will be dynamically stable under 10 GPa if they are synthesized in a proper way. In addition, we can expect that the hydrides are stable under higher pressures than 10 GPa since their crystal structures are derived from the DTSPs.

It is also worth mentioning that the  $(12-1-2-1)_V$  structure is isotypic to the  $Pm\bar{3}$  structure of  $ScYH_6$  (cP8) [36]. Importantly, the previous study indicated that cP8- $ScYH_6$  may possess the lowest enthalpy in the pressure range of 50–150 GPa [36]. Since several quaternary hydrides listed in Table II are the superstructures of cP8- $ScYH_6$ , we can expect that they may also have the lowest enthalpies under higher pressures. Note that the structure of cP8- $ScYH_6$  is the same as those of  $MgSiH_6$  [21] and  $MgGeH_6$  [22].

### C. Dynamic stability under 0 GPa

We additionally confirm the dynamic stability of  $H_{12}ScY_2Ca$  under 0 GPa by phonon dispersion and NPTMD. The result is consistent with the previous study that shows the dynamical stability of cP8- $ScYH_6$  under 0.01 GPa [36]. Since the lattice constant under 10 GPa is not so different from that under 0 GPa, we can expect that many stable hydrides discussed in Sec. III A will show dynamic stability under not only 10 GPa but also 0 GPa.

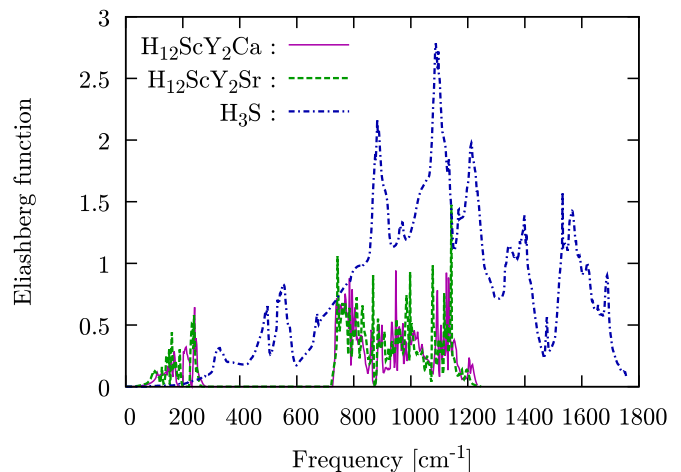


FIG. 9. Eliashberg function  $\alpha^2F(\omega)$  of  $H_{12}ScY_2Ca$  (magenta solid line),  $H_{12}ScY_2Sr$  (green dashed line), and  $H_3S$  (blue dash-dotted line).

### D. Superconductivity

We finally discuss the candidates of superconductors among the stable quaternary hydrides discovered in the study. Since the numerical cost to estimate  $T_c$  is considerable, we pick only two target hydrides up from the stable ones, namely,  $H_{12}ScY_2Ca$  and  $H_{12}ScY_2Sr$ . The guideline for the selection is as follows: (a) small SEF, (b) metallic electronic structure, and (c) hole-doped system to locate the Fermi level in the hydrogen bands. Table IV shows the calculated density of states per atom and per spin at the Fermi level  $D(\varepsilon_F)$ , electron-phonon mass-enhancement factor [85]

$$\lambda = 2 \int d\omega \frac{1}{\omega} \alpha^2 F(\omega), \quad (6)$$

averaged phonon frequency

$$\omega_{ln} = \exp\left(\frac{2}{\lambda} \int d\omega \frac{\ln \omega}{\omega} \alpha^2 F(\omega)\right), \quad (7)$$

and the superconducting transition temperature  $T_c$  without (wo) and with (w) the the spin fluctuation, where

$$\alpha^2 F(\omega) = \frac{1}{2\pi D(\varepsilon_F) N_a} \sum_{q\nu} \delta(\omega - \omega_{q\nu}) \frac{\gamma_{q\nu}}{\omega_{q\nu}} \quad (8)$$

is the Eliashberg function,  $N_a$  is the number of atoms in the unit cell, and  $\omega_{q\nu}$  and  $\gamma_{q\nu}$  are the phonon frequency and linewidth originating the electron-phonon coupling, respectively. We also compute those quantities of  $H_3S$  at a pressure of 200 GPa ( $Im\bar{3}m$  phase). By considering that the calculated  $T_c$  (190 K) of  $H_3S$  at 200 GPa is well compared to that (184 K) by the experiment [86], the calculated  $T_c$  for the new hydrides at 10 GPa is considered to be reliable. It is found that both the hydrides of  $H_{12}ScY_2Ca$  and  $H_{12}ScY_2Sr$  are superconductors with  $T_c$  of 5.7 and 6.7 K, respectively. Compared to  $T_c$  of  $H_3S$  at 200 GPa, the relatively lower  $T_c$  of the new hydrides can be traced back to the phononic properties of these materials. Figure 9 shows the Eliashberg function  $\alpha^2F(\omega)$  of  $H_{12}ScY_2Ca$ ,  $H_{12}ScY_2Sr$  (at 10 GPa), and  $H_3S$  (at 200 GPa).  $H_3S$  has a higher phonon frequency because of the compressed structure. These high-energy phonons create a wide energy window of

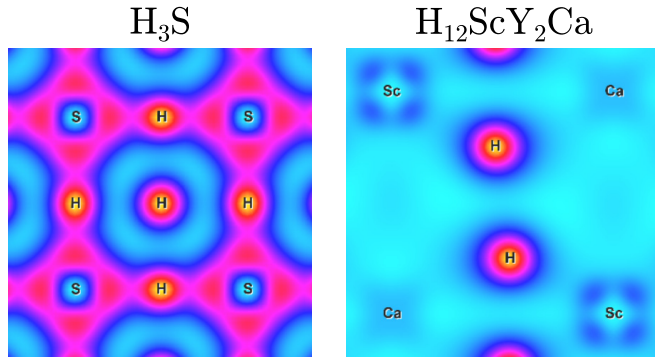


FIG. 10. Local density of states integrated between  $-1$  and  $1$  eV measured from the Fermi level in  $\text{H}_3\text{S}$  and  $\text{H}_{12}\text{ScY}_2\text{Ca}$ . Cyan, magenta, and yellow indicate low, medium, and high density, respectively.

the superconducting electrons and enhance  $\omega_{\text{ln}}$ . In  $\text{H}_{12}\text{ScY}_2\text{Ca}$  and  $\text{H}_{12}\text{ScY}_2\text{Sr}$  at 10 GPa, the interatomic force is small because of the ionic nature and phonon frequency is relatively low. Another reason for the lower  $T_c$  is the weak electron-phonon interaction in  $\text{H}_{12}\text{ScY}_2\text{Ca}$  and  $\text{H}_{12}\text{ScY}_2\text{Sr}$ . Although the density of states is comparable for these three materials,  $\lambda$  is much larger in  $\text{H}_3\text{S}$ . This difference of  $\lambda$  means the electron-phonon vertex is small in these quaternary hydrides. To analyze the reason for the weakness in the vertex, in Fig. 10, we plot the local density of states integrated between  $-1$  and  $1$  eV measured from the Fermi level. In  $\text{H}_3\text{S}$  at 200 GPa, the electronic states near the Fermi level locate on hydrogen atoms and the interatomic region. These electronic states are affected largely by the deformation potential for phonons that modulate H-S bonds. In  $\text{H}_{12}\text{ScY}_2\text{Ca}$ , electronic states around the Fermi level localize on the hydrogen atom. In this case, phonons hardly affect electronic states. If we increase the pressure to make hydrogen-atomic orbitals overlap, the electron-phonon coupling will increase because these interatomic states are affected by the bond-stretching mode.

#### IV. CONCLUSIONS

A few of the 60 kinds of PDTSPs have high symmetries and unique structural properties [50,51]. In this study, we focused on the (13-2-1) and (13-3-1) PDTSP structures, which can be utilized to derive the quaternary structural prototypes named (12-1-2-1) and (12-1-3-1) structures by substituting one small sphere in a cluster consisting of 13 small spheres with a fourth sphere. Substituting the small spheres in the two prototypes with hydrogen atoms gives unconventional hydrogen sublattices in cubic systems. Based on the two prototypes, we exhaustively searched the quaternary metal hydrides from 73 304 kinds of candidates. First, we excluded unstable hydrides by geometrical optimizations and NVTMDs. In this process, almost all the candidates generated from the (12-1-2-1) structure do not prefer their original structure but another one with the  $Fm\bar{3}$  symmetry named (12-1-2-1) $_V$  structure. Second, we calculated the SEFs including spin polarization to estimate the static stability. We found that the (12-1-2-1) $_V$ -type hydrides tend to have lower SEFs than the other two types of hydrides. Third, to confirm the dynamic stability of hydrides that have lower SEFs and no spin polarization,

we calculated the phonon dispersions of four kinds of (12-1-2-1)-type hydrides, 18 kinds of (12-1-2-1) $_V$ -type hydrides, and 6 kinds of (12-1-3-1)-type hydrides. As a result, one  $\text{H}_{12}\text{TiSc}_2\text{Cs}$  among the (12-1-2-1)-type hydrides, 16 hydrides among the (12-1-2-1) $_V$ -type hydrides, and all of the (12-1-3-1)-type hydrides show the dynamic stability. In addition, the NPTMDs for the 28 hydrides support the dynamic stability of the hydrides in most cases as well as the results of the phonon calculations. Among the hydrides with the dynamic stability, several hydrides including  $\text{H}_{12}\text{ScY}_2\text{Ca}$  have large gaps in phonon bands, high phonon frequency modes of hydrogen atoms, and a large H-PDOS near the Fermi level. From the similarities with several cubic hydrides such as  $\text{YH}_6$  and  $\text{LaH}_{10}$ , which are high-temperature SCs under high pressures [11,12], one may expect that their hydrogen sublattices are predominantly responsible for superconductivity with a high critical temperature. To predict the superconducting properties of the hydrides, we performed the SCDFT calculations including the plasmonic effect and spin fluctuation, and obtained the critical temperature  $T_c$  of 5.7 and 6.7 K for  $\text{H}_{12}\text{ScY}_2\text{Ca}$  and  $\text{H}_{12}\text{ScY}_2\text{Sr}$ , respectively. Although the obtained  $T_c$ 's are lower than those for the other cubic hydrides  $\text{YH}_6$  and  $\text{LaH}_{10}$ , it has been proven that our search based on PDTSPs is effective for discovering SCs with nontrivial cage structures consisting of hydrogen atoms in the crystal structure.

Not only the (13-2-1) and (13-3-1) structures but also some of the PDTSPs including the (9-6-3), (9-7-3), and (10-6-3), being understood as derivative structures of perovskite, and the (4-3-1) structure, being understood as a derivative structure of the  $\text{CaCu}_5$  structure, have high symmetries and unique structures that are difficult to design based on the perspectives of chemical bonds and/or local polyhedrons found in transition elements. We expect that such structural prototypes can help discover novel crystal structures, especially under high pressure. In addition, some of the local structures in the PDTSPs might be useful as the building blocks in crystals to design unknown structural prototypes [40,51]. While the predicted hydrides in the study may not be the most stable compound in their composition as discussed in Sec. III B, the 23 candidate compounds screened by the exhaustive search for 73 304 hydrides provide a guideline to narrow down the search space for trials in the experimental synthesis of quaternary metal hydrides.

#### ACKNOWLEDGMENTS

R.K. is financially supported by the Quantum Science and Technology Fellowship Program (Q-STEP) that is the University Fellowship program for Science and Technology Innovations, and the Grant-in-Aid for JSPS Research Fellow. The computations in this study have been done using the facilities (supercomputer Ohtaka) of the Supercomputer Center, the Institute for Solid State Physics, the University of Tokyo and also using the Fujitsu PRIMERGY CX400M1/CX2550M5 (Oakbridge-CX) at the Information Technology Center, The University of Tokyo. M.K. was supported by KAKENHI 20K15012. The authors would like to thank Masanobu Miyata and Mikio Koyano for kindly advising on how to use the ALAMODE code to calculate phonon properties.

- [1] A. R. Oganov and C. W. Glass, *J. Chem. Phys.* **124**, 244704 (2006).
- [2] A. R. Oganov, A. O. Lyakhov, and M. Valle, *Acc. Chem. Res.* **44**, 227 (2011).
- [3] A. O. Lyakhov, A. R. Oganov, H. T. Stokes, and Q. Zhu, *Comput. Phys. Commun.* **184**, 1172 (2013).
- [4] A. R. Oganov, Y. Ma, A. O. Lyakhov, M. Valle, and C. Gatti, *Rev. Mineral. Geochem.* **71**, 271 (2010).
- [5] *Computational Materials Discovery*, edited by A. R. Oganov, G. Saleh, and A. G. Kvashnin (The Royal Society of Chemistry, London, 2019).
- [6] Y. Wang, J. Lv, L. Zhu, and Y. Ma, *Phys. Rev. B* **82**, 094116 (2010).
- [7] Y. Wang, J. Lv, L. Zhu, and Y. Ma, *Comput. Phys. Commun.* **183**, 2063 (2012).
- [8] H. Wang, Y. Wang, J. Lv, Q. Li, L. Zhang, and Y. Ma, *Comput. Mater. Sci.* **112**, 406 (2016).
- [9] C. J. Pickard and R. J. Needs, *Phys. Rev. Lett.* **97**, 045504 (2006).
- [10] C. J. Pickard and R. J. Needs, *J. Phys.: Condens. Matter* **23**, 053201 (2011).
- [11] F. Peng, Y. Sun, C. J. Pickard, R. J. Needs, Q. Wu, and Y. Ma, *Phys. Rev. Lett.* **119**, 107001 (2017).
- [12] H. Liu, I. I. Naumov, R. Hoffmann, N. W. Ashcroft, and R. J. Hemley, *Proc. Natl. Acad. Sci. U.S.A.* **114**, 6990 (2017).
- [13] Z. M. Geballe, H. Liu, A. K. Mishra, M. Ahart, M. Somayazulu, Y. Meng, M. Baldini, and R. J. Hemley, *Angew. Chem., Int. Ed.* **57**, 688 (2018).
- [14] A. P. Drozdov, P. P. Kong, V. S. Minkov, S. P. Besedin, M. A. Kuzovnikov, S. Mozaffari, L. Balicas, F. F. Balakirev, D. E. Graf, V. B. Prakapenka, E. Greenberg, D. A. Knyazev, M. Tkacz, and M. I. Eremets, *Nature (London)* **569**, 528 (2019).
- [15] M. Somayazulu, M. Ahart, A. K. Mishra, Z. M. Geballe, M. Baldini, Y. Meng, V. V. Struzhkin, and R. J. Hemley, *Phys. Rev. Lett.* **122**, 027001 (2019).
- [16] V. Struzhkin, B. Li, C. Ji, X.-J. Chen, V. Prakapenka, E. Greenberg, I. Troyan, A. Gavriluk, and H.-k. Mao, *Matter Radiat. Extremes* **5**, 028201 (2020).
- [17] I. A. Troyan, D. V. Semenov, A. G. Kvashnin, A. V. Sadakov, O. A. Sobolevskiy, V. M. Pudalov, A. G. Ivanova, V. B. Prakapenka, E. Greenberg, A. G. Gavriluk, I. S. Lyubutin, V. V. Struzhkin, A. Bergara, I. Errea, R. Bianco, M. Calandra, F. Mauri, L. Monacelli, R. Akashi, and A. R. Oganov, *Adv. Mater.* **33**, 2006832 (2021).
- [18] Y. Sun, J. Lv, Y. Xie, H. Liu, and Y. Ma, *Phys. Rev. Lett.* **123**, 097001 (2019).
- [19] Y. Ge, F. Zhang, and Y. Yao, *Phys. Rev. B* **93**, 224513 (2016).
- [20] S. Zhang, L. Zhu, H. Liu, and G. Yang, *Inorg. Chem.* **55**, 11434 (2016).
- [21] Y. Ma, D. Duan, Z. Shao, H. Yu, H. Liu, F. Tian, X. Huang, D. Li, B. Liu, and T. Cui, *Phys. Rev. B* **96**, 144518 (2017).
- [22] Y. Ma, D. Duan, Z. Shao, D. Li, L. Wang, H. Yu, F. Tian, H. Xie, B. Liu, and T. Cui, *Phys. Chem. Chem. Phys.* **19**, 27406 (2017).
- [23] M. Rahm, R. Hoffmann, and N. W. Ashcroft, *J. Am. Chem. Soc.* **139**, 8740 (2017).
- [24] B. Liu, W. Cui, J. Shi, L. Zhu, J. Chen, S. Lin, R. Su, J. Ma, K. Yang, M. Xu, J. Hao, A. P. Durajski, J. Qi, Y. Li, and Y. Li, *Phys. Rev. B* **98**, 174101 (2018).
- [25] M. Amsler, *Phys. Rev. B* **99**, 060102(R) (2019).
- [26] X. Liang, A. Bergara, L. Wang, B. Wen, Z. Zhao, X.-F. Zhou, J. He, G. Gao, and Y. Tian, *Phys. Rev. B* **99**, 100505(R) (2019).
- [27] H. Xie, D. Duan, Z. Shao, H. Song, Y. Wang, X. Xiao, D. Li, F. Tian, B. Liu, and T. Cui, *J. Phys.: Condens. Matter* **31**, 245404 (2019).
- [28] X. Liang, S. Zhao, C. Shao, A. Bergara, H. Liu, L. Wang, R. Sun, Y. Zhang, Y. Gao, Z. Zhao, X.-F. Zhou, J. He, D. Yu, G. Gao, and Y. Tian, *Phys. Rev. B* **100**, 184502 (2019).
- [29] Z. Shao, D. Duan, Y. Ma, H. Yu, H. Song, H. Xie, D. Li, F. Tian, B. Liu, and T. Cui, *npj Comput. Mater.* **5**, 104 (2019).
- [30] P. Zhang, Y. Sun, X. Li, J. Lv, and H. Liu, *Phys. Rev. B* **102**, 184103 (2020).
- [31] S. Di Cataldo, W. von der Linden, and L. Boeri, *Phys. Rev. B* **102**, 014516 (2020).
- [32] W. Cui, T. Bi, J. Shi, Y. Li, H. Liu, E. Zurek, and R. J. Hemley, *Phys. Rev. B* **101**, 134504 (2020).
- [33] Y. Yan, T. Bi, N. Geng, X. Wang, and E. Zurek, *J. Phys. Chem. Lett.* **11**, 9629 (2020).
- [34] H.-Y. Lv, S.-Y. Zhang, M.-H. Li, Y.-L. Hai, N. Lu, W.-J. Li, and G.-H. Zhong, *Phys. Chem. Chem. Phys.* **22**, 1069 (2020).
- [35] S. Di Cataldo, C. Heil, W. von der Linden, and L. Boeri, *Phys. Rev. B* **104**, L020511 (2021).
- [36] Y. K. Wei, L. Q. Jia, Y. Y. Fang, L. J. Wang, Z. X. Qian, J. N. Yuan, G. Selvaraj, G. F. Ji, and D. Q. Wei, *Int. J. Quantum Chem.* **121**, e26459 (2021).
- [37] H. Liu, R. Cheng, K. Yang, B. Li, L. Chen, and W. Lu, *Phys. Lett. A* **390**, 127109 (2021).
- [38] P. Song, Z. Hou, P. B. d. Castro, K. Nakano, K. Hongo, Y. Takano, and R. Maezono, *Chem. Mater.* **33**, 9501 (2021).
- [39] S. Di Cataldo, W. von der Linden, and L. Boeri, *npj Comput. Mater.* **8**, 2 (2022).
- [40] Z. Zhang, T. Cui, M. J. Hutcheon, A. M. Shipley, H. Song, M. Du, V. Z. Kresin, D. Duan, C. J. Pickard, and Y. Yao, *Phys. Rev. Lett.* **128**, 047001 (2022).
- [41] X. Zhang, Y. Zhao, and G. Yang, *WIREs Comput. Mol. Sci.* **12**, e1582 (2022).
- [42] T. Muramatsu, W. K. Wanene, M. Somayazulu, E. Vinitsky, D. Chandra, T. A. Strobel, V. V. Struzhkin, and R. J. Hemley, *J. Phys. Chem. C* **119**, 18007 (2015).
- [43] D. Meng, M. Sakata, K. Shimizu, Y. Iijima, H. Saitoh, T. Sato, S. Takagi, and S.-i. Orimo, *Phys. Rev. B* **99**, 024508 (2019).
- [44] E. Snider, N. Dasenbrock-Gammon, R. McBride, M. Debessai, H. Vindana, K. Vencatasamy, K. V. Lawler, A. Salamat, and R. P. Dias, *Nature (London)* **586**, 373 (2020).
- [45] J. Bardeen, L. N. Cooper, and J. R. Schrieffer, *Phys. Rev.* **108**, 1175 (1957).
- [46] N. W. Ashcroft, *Phys. Rev. Lett.* **92**, 187002 (2004).
- [47] N. W. Ashcroft, *Phys. Rev. Lett.* **21**, 1748 (1968).
- [48] C. F. Richardson and N. W. Ashcroft, *Phys. Rev. Lett.* **78**, 118 (1997).
- [49] R. P. Dias and I. F. Silvera, *Science* **355**, 715 (2017).
- [50] R. Koshiji and T. Ozaki, *Phys. Rev. E* **104**, 024101 (2021).
- [51] R. Koshiji and T. Ozaki, *J. Phys. Commun.* **6**, 075002 (2022).
- [52] R. Koshiji, M. Kawamura, M. Fukuda, and T. Ozaki, *Phys. Rev. E* **103**, 023307 (2021).
- [53] M. Rahm, R. Cammi, N. W. Ashcroft, and R. Hoffmann, *J. Am. Chem. Soc.* **141**, 10253 (2019).
- [54] K. Momma and F. Izumi, *J. Appl. Crystallogr.* **44**, 1272 (2011).
- [55] A. B. Hopkins, Y. Jiao, F. H. Stillinger, and S. Torquato, *Phys. Rev. Lett.* **107**, 125501 (2011).



- [56] A. B. Hopkins, F. H. Stillinger, and S. Torquato, *Phys. Rev. E* **85**, 021130 (2012).
- [57] T. Ozaki, *Phys. Rev. B* **67**, 155108 (2003).
- [58] T. Ozaki and H. Kino, *Phys. Rev. B* **69**, 195113 (2004).
- [59] T. Ozaki and H. Kino, *Phys. Rev. B* **72**, 045121 (2005).
- [60] T. Ozaki, H. Kino, J. Yu, M. J. Han, N. Kobayashi, M. Ohfuti, F. Ishii, T. Ohwaki, H. Weng, K. Terakura, 2009, <http://www.openmx-square.org/>.
- [61] J. P. Perdew, K. Burke, and M. Ernzerhof, *Phys. Rev. Lett.* **77**, 3865 (1996).
- [62] W. Kohn and L. J. Sham, *Phys. Rev.* **140**, A1133 (1965).
- [63] See Supplemental Material at <http://link.aps.org/supplemental/10.1103/PhysRevMaterials.6.114802> for details of pseudoatomic orbital basis functions, phonon properties, band structures, and the hydrides that show the dynamical stabilities in NVTMDs.
- [64] A. Banerjee, N. Adams, J. Simons, and R. Shepard, *J. Phys. Chem.* **89**, 52 (1985).
- [65] S. Nosé, *J. Chem. Phys.* **81**, 511 (1984).
- [66] S. Nosé, *Mol. Phys.* **52**, 255 (1984).
- [67] W. G. Hoover, *Phys. Rev. A* **31**, 1695 (1985).
- [68] L. Woodcock, *Chem. Phys. Lett.* **10**, 257 (1971).
- [69] M. Parrinello and A. Rahman, *Phys. Rev. Lett.* **45**, 1196 (1980).
- [70] T. Tadano, Y. Gohda, and S. Tsuneyuki, *J. Phys.: Condens. Matter* **26**, 225402 (2014).
- [71] A. Togo and I. Tanaka, [arXiv:1808.01590](https://arxiv.org/abs/1808.01590).
- [72] U. Müller, Linked polyhedra, in *Inorganic Structural Chemistry* (Wiley, New York, 2006), Chap. 16, pp. 166–189.
- [73] B. Cordero, V. Gómez, A. E. Platero-Prats, M. Revés, J. Echeverría, E. Cremades, F. Barragán, and S. Alvarez, *Dalton Trans.* **2008**, 2832 (2008).
- [74] M. Lüders, M. A. L. Marques, N. N. Lathiotakis, A. Floris, G. Profeta, L. Fast, A. Continenza, S. Massidda, and E. K. U. Gross, *Phys. Rev. B* **72**, 024545 (2005).
- [75] P. Giannozzi, O. Andreussi, T. Brumme, O. Bunau, M. B. Nardelli, M. Calandra, R. Car, C. Cavazzoni, D. Ceresoli, M. Cococcioni *et al.*, *J. Phys.: Condens. Matter* **29**, 465901 (2017).
- [76] A. Sanna, C. Pellegrini, and E. K. U. Gross, *Phys. Rev. Lett.* **125**, 057001 (2020).
- [77] R. Akashi and R. Arita, *Phys. Rev. Lett.* **111**, 057006 (2013).
- [78] A. Davydov, A. Sanna, C. Pellegrini, J. K. Dewhurst, S. Sharma, and E. K. U. Gross, *Phys. Rev. B* **102**, 214508 (2020).
- [79] F. Essenberg, A. Sanna, A. Linscheid, F. Tandetzy, G. Profeta, P. Cudazzo, and E. K. U. Gross, *Phys. Rev. B* **90**, 214504 (2014).
- [80] M. Kawamura, Y. Hizume, and T. Ozaki, *Phys. Rev. B* **101**, 134511 (2020).
- [81] M. Kawamura, Y. Gohda, and S. Tsuneyuki, *Phys. Rev. B* **89**, 094515 (2014).
- [82] G. Prandini, A. Marrazzo, I. E. Castelli, N. Mounet, and N. Marzari, *npj Comput. Mater.* **4**, 72 (2018).
- [83] The three-dimensional data of the hydrides discussed in this study are available on the website of <http://www.samlai-square.org/>.
- [84] A. Jain, S. P. Ong, G. Hautier, W. Chen, W. D. Richards, S. Dacek, S. Cholia, D. Gunter, D. Skinner, G. Ceder, and K. A. Persson, *APL Mater.* **1**, 011002 (2013).
- [85] W. L. McMillan, *Phys. Rev.* **167**, 331 (1968).
- [86] A. P. Drozdov, M. I. Erements, I. A. Troyan, V. Ksenofontov, and S. I. Shylin, *Nature (London)* **525**, 73 (2015).